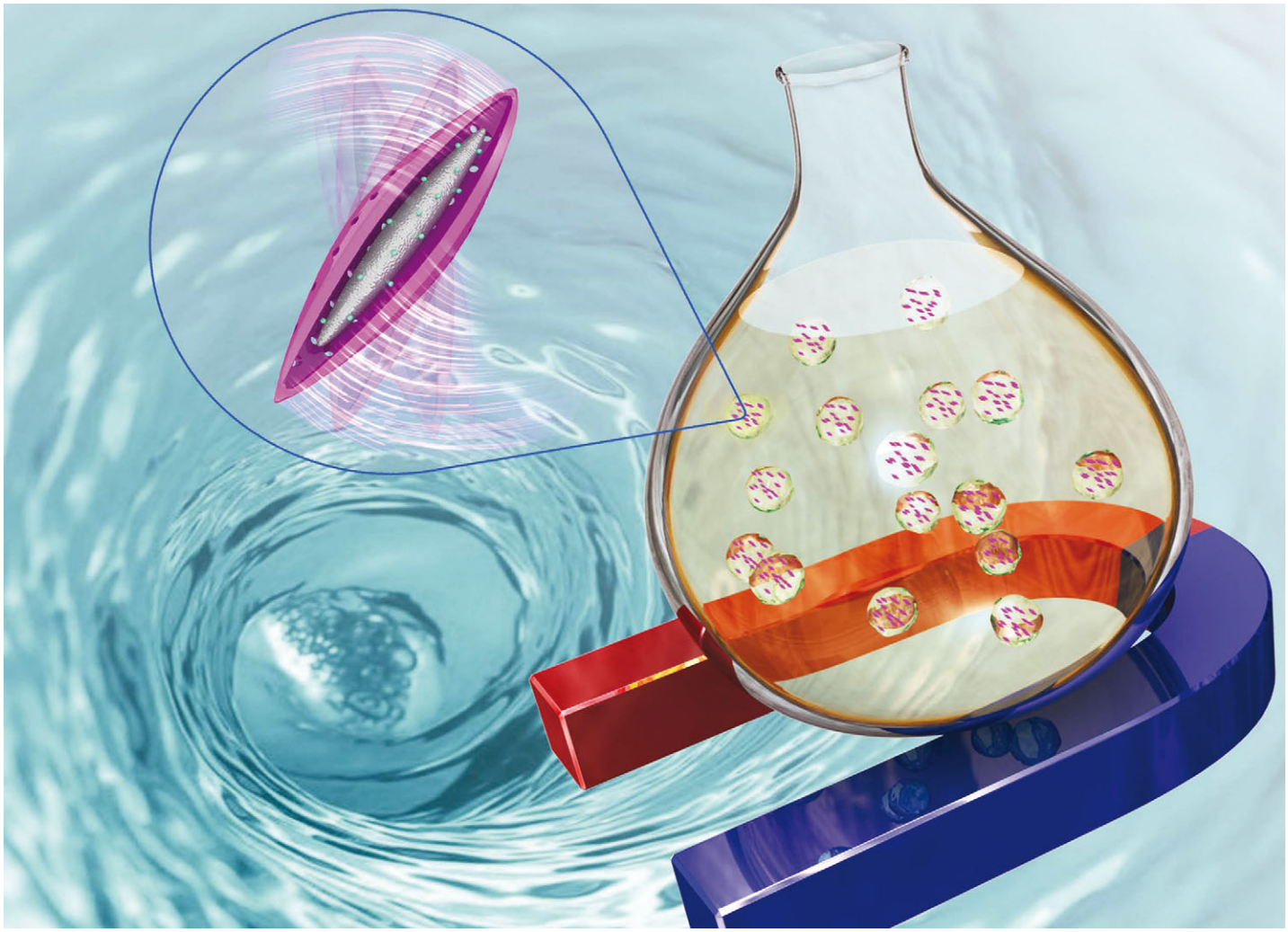

Showcasing the work of Prof. Weiguo Song at the Beijing National Laboratory for Molecular Sciences, Laboratory of Molecular Nanostructures and Nanotechnology, Institute of Chemistry, Chinese Academy of Sciences, Beijing, China.

Spindle-shaped nanoscale yolk/shell magnetic stirring bars for heterogeneous catalysis in macro- and microscopic systems

A new type of spindle-shaped Pd–Fe@*meso*-SiO_2 yolk/shell nanoscale magnetic stirring bar containing noble metal nanoparticles is prepared. It not only shows impressive activity and stability as a heterogeneous catalyst in a macroscopic flask system, but also acts as an efficient nanoscale magnetic stirrer in a microscopic droplet system.

As featured in:

See Changyan Cao, Weiguo Song *et al.*, *Chem. Commun.*, 2016, **52**, 1575.

ROYAL SOCIETY OF CHEMISTRY

www.rsc.org/chemcomm

Registered charity number: 207890

ChemComm

COMMUNICATION

View Article Online
View Journal | View Issue

Cite this: *Chem. Commun.*, 2016, 52, 1575

Received 3rd November 2015,
Accepted 10th November 2015

DOI: 10.1039/c5cc09104g

www.rsc.org/chemcomm

Spindle-shaped nanoscale yolk/shell magnetic stirring bars for heterogeneous catalysis in macro- and microscopic systems†

Shuliang Yang,[a] Changyan Cao,*[a] Li Peng,[b] Peipei Huang,[a] Yongbin Sun,[a] Fang Wei[a] and Weiguo Song*[a]

A new type of spindle-shaped nanoscale yolk/shell magnetic stirring bar containing noble metal nanoparticles was prepared. The as-synthesized Pd–Fe@meso-SiO_2 not only showed impressive activity and stability as a heterogeneous catalyst in a macroscopic flask system, but also acted as an efficient nanoscale magnetic stir bar in a microscopic droplet system.

Hybrid nanocomposites with yolk/shell nanostructures have shown exciting features as heterogeneous catalysts.[1] Compared with the traditionally supported catalysts, yolk/shell nanostructured catalysts have two distinguished features: one is faster reaction rate because of the confinement effect in the nanoreactors;[2] and the other one is better catalytic stability.[3] The outer shells could prevent the aggregation and leaching of active species. The highly tunable structure of shell and yolk, including the composition, the pore size of the shell, and the space between yolk and the shell, opens up a new avenue for the controllable synthesis of heterogeneous catalysts with a particular catalytic performance.[4] For example, through the adjustment of the pore size of the porous shell, shape-selective catalysis in liquid solutions can be obtained.[5] The chemoselectivity of organic reactions could also be improved significantly through the adjustment of the strong interactions between the noble metals and shells.[5a,6]

In another aspect of catalysis, rapid mass transfer is very important for heterogeneous catalysis in a liquid reaction system, which determines the reaction rate and catalytic activity of catalysts. In order to enhance the mass transportation efficiency, researchers mainly focus on the design of nanostructures of catalysts, such as core/shell or yolk/shell nanoreactors. One easily neglectable but very important fact is that magnetic or mechanical stirring is still used in most liquid reaction systems for obtaining better mixing and faster mass transportation. However, this kind of traditional stirring technology cannot be used in tiny liquid reactors, such as microdroplets, which are of great importance for lab-on-chip applications and microliter bioassay.[7] In addition, the structures of many fragile catalysts such as flowerlike MgO might be destroyed under vigorous traditional stirring, resulting in poor stability.[8] The development of nanoscale magnetic stirring bars that are sufficiently small but still able to transduce external energy for mixing is an efficient way to solve the above-mentioned problems.

In our previous work, we reported nanoscale magnetic stirring bars containing Pd nanoparticles for heterogeneous catalysis for the first time.[9] As a part of our continuing work, we herein developed a facile method to prepare a new kind of spindle-like nanoscale yolk/shell magnetic stirring bars containing noble metal nanoparticles for heterogeneous catalysis in a macroscopic flask and microscopic droplets. Because the density of Fe(0) is higher than the α-Fe_2O_3, when α-Fe_2O_3 was reduced to Fe(0) during the H_2-reduction procedure, Fe(0) would occupy a smaller volume. Thus, a void space was formed between the SiO_2 shell and the Fe core. Through this route, the Pd–Fe@meso-SiO_2 yolk/shell nanostructure was prepared successfully and the use of a sacrificial template was avoided completely. Due to the protection of the SiO_2 shell, interference from the outside environment could be decreased effectively, which is beneficial for the alleviation of noble-metal nanoparticles aggregation. Moreover, the noble metal leaching could be avoided efficiently due to the reducibility of the metallic Fe core. Last but not least, with the magnetic response of the spindle-shaped yolk/shell nanostructures, the prepared Pd–Fe@meso-SiO_2 could also be used as a nanoscale magnetic stirring bar to speed up mass transfer in microscopic systems.

The preparation process is illustrated in Scheme 1a. The procedure for preparing nanoscale Pd–Fe@meso-SiO_2 yolk/shell magnetic stirring bars can be divided into four steps. Firstly, α-Fe_2O_3 spindles were prepared according to our previous report.[4a] In the second step, with the assistance of tetraethoxysilane (TEOS), (1-hexadecyl)trimethyl ammonium bromide (CTAB) and polyvinylpyrrolidone (PVP, K-30), a mesoporous SiO_2 coating was formed

[a] *Beijing National Laboratory for Molecular Sciences, Laboratory of Molecular Nanostructures and Nanotechnology, Institute of Chemistry, Chinese Academy of Sciences, 100190, Beijing, China. E-mail: cycao@iccas.ac.cn, wsong@iccas.ac.cn; Fax: +86-10-62557908; Tel: +86-10-62557908*

[b] *École Polytechnique Fédérale de Lausanne (EPFL), Institute of Chemical Sciences and Engineering, EPFL-ISIC-Valais, Sion, Switzerland*

† Electronic supplementary information (ESI) available: Materials, experimental details, and characterization. See DOI: 10.1039/c5cc09104g

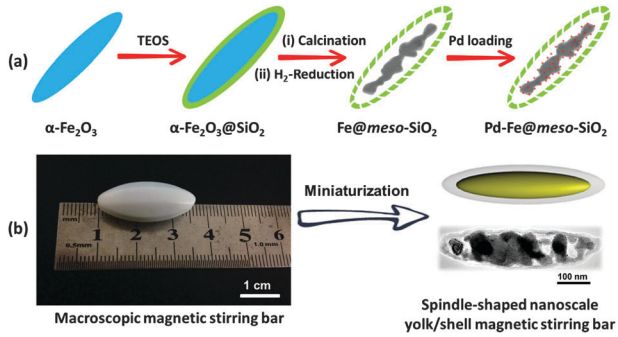

Scheme 1 (a) Schematic illustration for the preparation procedure of nanoscale Pd–Fe@meso-SiO_2 yolk/shell magnetic stirring bars. (b) Miniaturization of the macroscopic magnetic stirring bar towards the nanoscale spindle-shaped Pd–Fe@meso-SiO_2 yolk/shell magnetic stirring bar.

outside the spindle α-Fe_2O_3.[4a,8,10] The third step could be divided into two small consecutive steps. The surfactants were first removed through calcination in air to produce mesoporous SiO_2 shells, and then the inner α-Fe_2O_3 cores were reduced to Fe under a H_2 atmosphere. Finally, the noble metal Pd nanoparticles were formed through a simple *in situ* galvanic replacement reaction between the Fe core and Na_2PdCl_4 ($E_{Fe^{2+}/Fe}$ = −0.44 V *vs.* $E_{PdCl_4^{2-}/Pd}$ = +0.62 V). The XRD patterns of all the samples obtained at different steps also confirmed that each experimental step was pushed forward successfully (Fig. 1).

Fig. 2a and Fig. S1a (ESI†) show that the as-prepared spindle-shaped α-Fe_2O_3 particles had a uniform size. After SiO_2 coating, a *ca.* 15 nm thickness layer could be seen clearly from the TEM images (Fig. 2b and Fig. S1b, ESI†). After the reduction process, the α-Fe_2O_3 core was reduced to magnetic Fe (Fig. 1c). At the same time, the void space between the SiO_2 shell and the Fe core can be produced (Fig. 2c) due to the density difference between α-Fe_2O_3 and Fe. Using such a design, the use of sacrificial template was avoided, resulting in this method being a facile one to prepare a yolk/shell nanoreactor. From the ICP-AES analysis, the Fe content

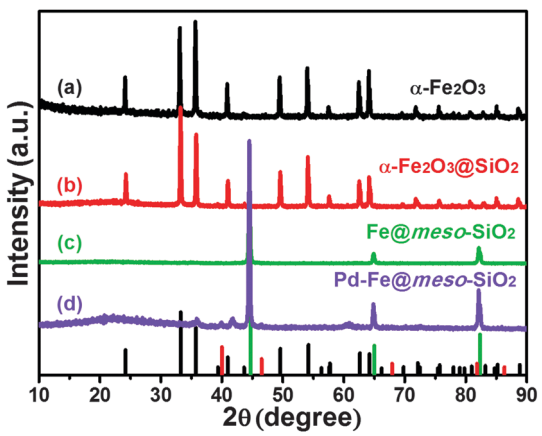

Fig. 1 XRD patterns of α-Fe_2O_3 nanospindles (a), α-Fe_2O_3@SiO_2 (b), Fe@meso-SiO_2 (c) and Pd–Fe@meso-SiO_2 (d). Dark lines, green lines and red lines at the bottom were the standard PDF cards of α-Fe_2O_3 (JCPDS No. 89-8103), Fe (JCPDS No. 06-0696) and Pd (JCPDS No. 88-2335), respectively.

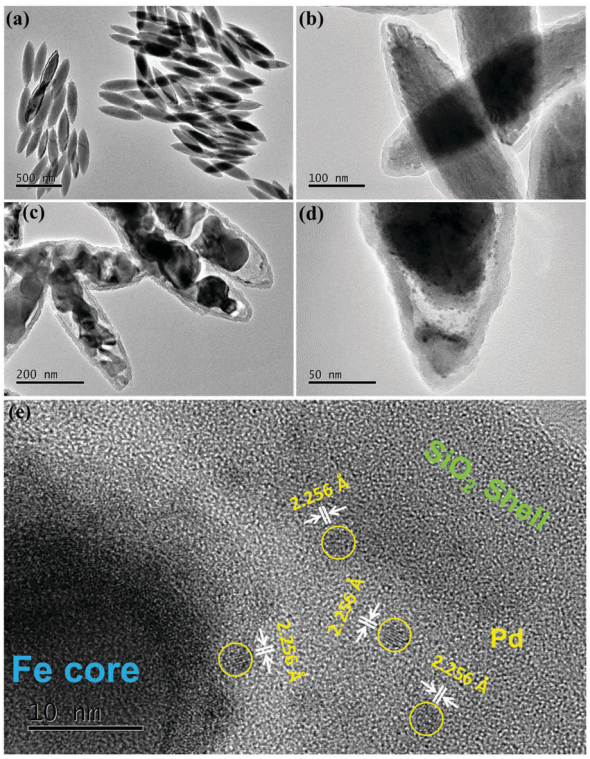

Fig. 2 TEM images of α-Fe_2O_3 nanospindles (a), α-Fe_2O_3@SiO_2 (b), Fe@meso-SiO_2 (c) and Pd–Fe@meso-SiO_2 (d and e).

in the Fe@meso-SiO_2 was 72.6 wt%. As the standard electrode potential of the Fe^{2+}/Fe pair ($E_{Fe^{2+}/Fe}$ = −0.44 V) is much lower than that of many noble metal ion/metal pairs, the galvanic displacement reaction between Fe and noble metal ions can take place easily. At the same time, because the reducing agent (Fe core) remained inside the shell, it could ensure that the galvanic replacement reaction took place just inside the shell. From the TEM image, all of the Pd nanoparticles (NPs) were indeed loaded inside the SiO_2 shell and no Pd NPs were observed on the outside of the shell (Fig. 2d). The diameter of Pd NPs was only about 2.0 nm. The Pd content in the Pd–Fe@meso-SiO_2 was 2.7 wt% from ICP-AES analysis. The crystal lattice of Pd could be clearly observed in the HRTEM image (Fig. 2e). In addition, elemental mapping of the Pd–Fe@meso-SiO_2 nanostructures also confirmed that Fe, O, Si and Pd elements were distributed uniformly (Fig. S2, ESI†). The small-angle XRD pattern of the Pd–Fe@meso-SiO_2 showed a broad peak at 1.5° with a low intensity, indicating worm-like disordered mesopores with a uniform pore size (Fig. S3, ESI†).[11] Other noble metal–Fe@meso-SiO_2 composites, including Pt–Fe@meso-SiO_2 and Au–Fe@meso-SiO_2, could also be obtained successfully and all the noble metal nanoparticles were loaded inside the SiO_2 shell (Fig. S4, ESI†).

As shown in Fig. 3, N_2 adsorption/desorption isotherms of Pd–Fe@meso-SiO_2 exhibited a typical type IV isotherm, which revealed the characteristics of mesoporous materials.[12] The pore size distribution calculated using the DFT method showed a peak centered at around 3.4 nm (inset of Fig. 3), which should mainly arise from the mesoporous SiO_2 shell. Moreover, the sample had a Brunauer–Emmett–Teller (BET) surface area of 134.0 m^2 g^{-1}.

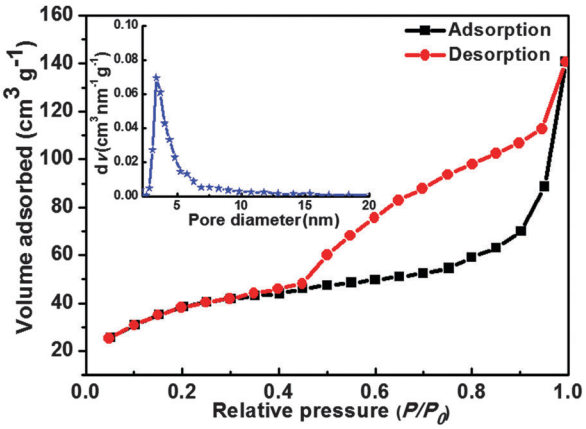

Fig. 3 N_2 adsorption/desorption isotherms of the Pd–Fe@meso-SiO_2. The inset shows the mesopore size distribution curve.

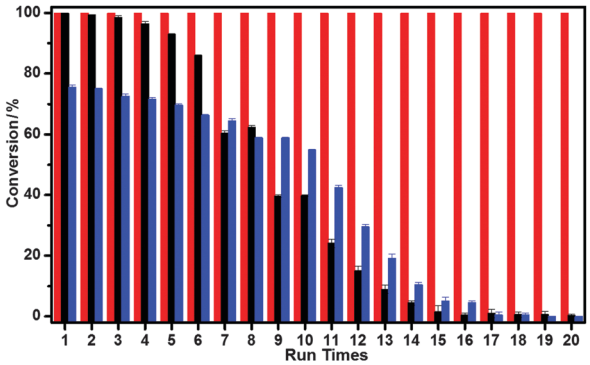

Fig. 4 Recycle performance of Pd–Fe@meso-SiO_2 (red), control sample Fe@meso-SiO_2/Pd (dark) and commercial Pd/C (blue) catalyst using styrene hydrogenation as the model reaction.

Due to the special features of Pd–Fe@meso-SiO_2, such as mesoporous channels, yolk/shell structure, and small size of Pd nanoparticles, we envisioned that they could be used as excellent heterogeneous catalysts. Palladium can dissolve 700 times the volume of hydrogen at room temperature, so Pd-based catalysts were often used in hydrogenation reactions,[13] such as hydrogenation of phenols,[14] olefins,[15] alkynes,[16] carboxyl/aldehyde hydrogenation,[17] and so on. Therefore, we chose the styrene hydrogenation in a macroscopic flask as a model reaction to test the catalytic properties of Pd–Fe@meso-SiO_2. As shown in Table 1, the substrate expansion results showed excellent catalytic activity of Pd–Fe@meso-SiO_2 for a variety of olefins. A hot extraction experiment confirmed that the catalysis was exclusively heterogeneous (Fig. S5, ESI†). For comparison, the commercially available Pd/C catalyst and Pd nanoparticles loaded on the outside of Fe@meso-SiO_2 (denoted as Fe@meso-SiO_2/Pd, with 3.9 wt% Pd loading, the detailed preparation procedures and characterization can be seen in the experimental section and Fig. S6, ESI†) were also prepared and tested. As displayed in Fig. 4, the catalytic activity of Pd–Fe@meso-SiO_2 was nearly the same as that of Fe@meso-SiO_2/Pd, but better than that of commercial Pd/C.

Table 1 Scope of the hydrogenation of olefins with Pd–Fe@meso-SiO_2[a]

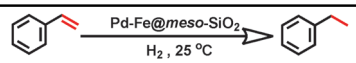

Entry	Olefin	Product	Time (min)	Conversion[b] [%]	TOF [h^{-1}]
1			15	>99	7883
2[c]			15	0	—
3	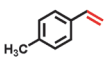	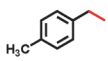	10	>99	11 824
4	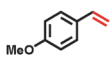	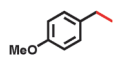	10	>99	11 824
5	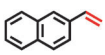	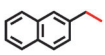	25	>99	4730
6			40	>99	2956
7[d]	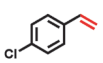	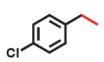	10	>99	11 824

[a] Reaction conditions: olefins (2.5 mmol), Pd–Fe@meso-SiO_2 (5.0 mg), ethanol (5 mL), 25 °C, under 1.0 MPa H_2 atmosphere. [b] Conversion was determined by GC, and the identity was ascertained by GC-MS. [c] 5.0 mg Fe@meso-SiO_2 was adopted as a catalyst. [d] No dechlorination product was detected and the selectivity for 1-chloro-4-ethylbenzene was above 99%.

Besides the excellent catalytic activity, Pd–Fe@meso-SiO_2 also showed impressive catalytic stability. As displayed in Fig. 4, even after being reused 20 times, no obvious loss of activity can be observed. However, after 20 runs, serious aggregations and detachments of Pd nanoparticles were observed for Fe@meso-SiO_2/Pd (Fig. S7, ESI†). The excellent catalytic stability of the as-prepared Pd–Fe@meso-SiO_2 should be ascribed to the following reasons: (i) the confinement effect of the yolk/shell nanostructures increased the local substrate concentration around Pd NPs, which speeded up the catalytic process; (ii) with the protection of the SiO_2 shell, Pd leaching could be avoided efficiently. After the 20th run, Pd loading of the recovered Pd–Fe@meso-SiO_2 was 2.5 wt% from ICP-AES analysis, which was very close to the original value (2.7 wt%). This result implied that the Pd leaching during the cycling process was negligible. (iii) After the 20th recycle, though the Pd NPs aggregation in the same shell happened to some extent (Fig. S8, ESI†), the aggregation of Pd NPs from different shells did not occur. In other words, the Pd NPs still remain inside the original SiO_2 shell, which could alleviate the Pd NPs aggregation efficiently. (iv) Due to the magnetism of the Fe core, the Pd–Fe@meso-SiO_2 could be easily recovered from the reaction solution using a magnet (Fig. S9, ESI†). This simplified the recovery procedure and avoided catalyst loss during the recycling process.

Due to the excess inner Fe core, another highlight of the Pd–Fe@meso-SiO_2 was that the content of Pd could be easily controlled through an additional volume of Na_2PdCl_4. For example, 5.0 wt% Pd could be loaded when two times the volume of Na_2PdCl_4 (100 μL) was used. From the XRD pattern, the Pd diffraction peaks of 5.0 wt% loading were more obvious than 2.7 wt% Pd loading (Fig. S10, ESI†). TEM images showed that all of the Pd NPs also stayed inside the shell (Fig. S11, ESI†). It is worth noting that loading all the noble metal

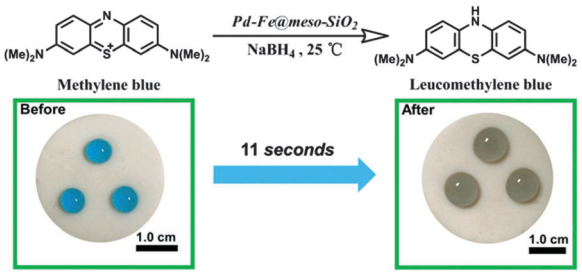

Fig. 5 Hydrogenation of methylene blue (MB) in microdroplets with Pd–Fe@meso-SiO_2 as a magnetic stirring bar and catalyst.

nanoparticles into the inside of the shell perfectly while maintaining a relatively small size is very hard to realize. In fact, the nanoparticles often block the pores of the mesoporous shell in a traditional impregnation method.[18]

Moreover, considering the spindle-shaped structure and magnetic features of Pd–Fe@meso-SiO_2, we envisioned that it may also be used as a nanoscale magnetic stirring bar in a microscopic system for better mixing of reactants (Scheme 1b).[9,19] The hydrogenation of methylene blue (MB) in microdroplets was chosen as a model reaction, because the color change of the blue MB solution is a direct indicator of the reaction progress. As shown in Fig. 5, the blue microdroplets became colorless in 11 s after addition of Pd–Fe@meso-SiO_2 (Video S1, ESI†). Moreover, the rotation of the Pd–Fe@meso-SiO_2 could be observed clearly when the magnetic stirring plate was turned on and off intermittently (Video S2, ESI†). In comparison, the fading rate of MB became much slower when the magnetic stirring plate was turned off even though the same amount of Pd–Fe@meso-SiO_2 was added (Video S3, ESI†). The faster reaction rate should be ascribed to the far better mixing under the rotation of Pd–Fe@meso-SiO_2 when the magnetic stirring plate was turned on.

In summary, a facile method was developed to prepare spindle-shaped nanoscale yolk/shell magnetic stirring bars. A void space between the yolk and the shell was formed during thermal treatment due to the density difference between α-Fe_2O_3 and Fe, and the sacrificial layer was avoided completely. Furthermore, the Pd, Pt and Au nanoparticles were deposited on the inside of the SiO_2 shell through the galvanic replacement reaction between the metallic Fe yolk and noble metal precursors. When used as heterogeneous catalysts for hydrogenation of olefins in a macroscopic flask, the as-prepared Pd–Fe@meso-SiO_2 showed impressive activity and stability. More interestingly, they could stir in the microscopic droplets under an external magnetic field to accelerate mass transfer, and displayed much better catalytic activity during the hydrogenation of methylene blue (MB) when compared with the reaction rate without stirring.

The authors thank the National Natural Science Foundation of China (Grants NSFC 21573244, 21333009, 21273244 and 51402305), and Chinese Academy of Sciences (Grant KJCX2-YW-N41) for financial support.

Notes and references

1 (*a*) Q. Zhang, I. Lee, J. B. Joo, F. Zaera and Y. Yin, *Acc. Chem. Res.*, 2012, **46**, 1816; (*b*) R. Ghosh Chaudhuri and S. Paria, *Chem. Rev.*, 2011, **112**, 2373; (*c*) M. Cargnello, J. J. D. Jaen, J. C. H. Garrido, K. Bakhmutsky, T. Montini, J. J. C. Gamez, R. J. Gorte and P. Fornasiero, *Science*, 2012, **337**, 713; (*d*) G.-H. Wang, J. Hilgert, F. H. Richter, F. Wang, H.-J. Bongard, B. Spliethoff, C. Weidenthaler and F. Schüth, *Nat. Mater.*, 2014, **13**, 293.

2 (*a*) M. Pérez-Lorenzo, B. Vaz, V. Salgueiriño and M. A. Correa-Duarte, *Chem. – Eur. J.*, 2013, **19**, 12196; (*b*) Y. Yang, M. Ambrogi, H. Kirmse, Y. Men, M. Antonietti and J. Yuan, *Chem. Mater.*, 2014, **27**, 127; (*c*) M. Presle, I. Maurin, F. Maroun, R. Cortès, L. Lu, R. Sayed Hassan, E. Larquet, J.-M. Guigner, E. Rivière, J. P. Wright, J.-P. Boilot and T. Gacoin, *J. Phys. Chem. C*, 2014, **118**, 13186.

3 (*a*) T. Mitsudome and K. Kaneda, *ChemCatChem*, 2013, **5**, 1681; (*b*) Z.-A. Qiao, P. Zhang, S.-H. Chai, M. Chi, G. M. Veith, N. C. Gallego, M. Kidder and S. Dai, *J. Am. Chem. Soc.*, 2014, **136**, 11260; (*c*) J. Peng, G. Lan, M. Guo, X. Wei, C. Li and Q. Yang, *Chem. – Eur. J.*, 2015, **21**, 10490; (*d*) J. Du, J. Qi, D. Wang and Z. Tang, *Energy Environ. Sci.*, 2012, **5**, 6914; (*e*) Y. Yao, X. Zhang, J. Peng and Q. Yang, *Chem. Commun.*, 2015, **51**, 3750; (*f*) K. Dong, Z. Liu and J. Ren, *CrystEngComm*, 2013, **15**, 6329.

4 (*a*) Z.-M. Cui, Z. Chen, C.-Y. Cao, L. Jiang and W.-G. Song, *Chem. Commun.*, 2013, **49**, 2332; (*b*) X. Wang, D. Liu, S. Song and H. Zhang, *J. Am. Chem. Soc.*, 2013, **135**, 15864.

5 (*a*) Y. Liu, W. Zhang, S. Li, C. Cui, J. Wu, H. Chen and F. Huo, *Chem. Mater.*, 2014, **26**, 1119; (*b*) S. Li, T. Boucheron, A. Tuel, D. Farrusseng and F. Meunier, *Chem. Commun.*, 2014, **50**, 1824.

6 (*a*) E. Weiss, B. Dutta, A. Kirschning and R. Abu-Reziq, *Chem. Mater.*, 2014, **26**, 4781; (*b*) T. Mitsudome, Y. Takahashi, S. Ichikawa, T. Mizugaki, K. Jitsukawa and K. Kaneda, *Angew. Chem., Int. Ed.*, 2013, **52**, 1481; (*c*) K. Qu, L. Wu, J. Ren and X. Qu, *Nano Res.*, 2013, **6**, 693.

7 (*a*) S. Haeberle and R. Zengerle, *Lab Chip*, 2007, **7**, 1094; (*b*) A. J. deMello, *Nature*, 2006, **442**, 394.

8 Z.-M. Cui, Z. Chen, C.-Y. Cao, W.-G. Song and L. Jiang, *Chem. Commun.*, 2013, **49**, 6093.

9 S. Yang, C. Cao, Y. Sun, P. Huang, F. Wei and W. Song, *Angew. Chem., Int. Ed.*, 2015, **54**, 2661.

10 H. Chen, D. Sulejmanovic, T. Moore, D. C. Colvin, B. Qi, O. T. Mefford, J. C. Gore, F. Alexis, S.-J. Hwu and J. N. Anker, *Chem. Mater.*, 2014, **26**, 2105.

11 Z. Chen, Z.-M. Cui, F. Niu, L. Jiang and W.-G. Song, *Chem. Commun.*, 2010, **46**, 6524.

12 J. C. Groen, L. A. A. Peffer and J. Pérez-Ramírez, *Microporous Mesoporous Mater.*, 2003, **60**, 1.

13 K. Qu, L. Wu, J. Ren and X. Qu, *ACS Appl. Mater. Interfaces*, 2012, **4**, 5001.

14 (*a*) Y. Wang, J. Yao, H. Li, D. Su and M. Antonietti, *J. Am. Chem. Soc.*, 2011, **133**, 2362; (*b*) H. Liu, Y. Li, R. Luque and H. Jiang, *Adv. Synth. Catal.*, 2011, **353**, 3107; (*c*) J.-F. Zhu, G.-H. Tao, H.-Y. Liu, L. He, Q.-H. Sun and H.-C. Liu, *Green Chem.*, 2014, **16**, 2664.

15 (*a*) R. Long, Z. Rao, K. Mao, Y. Li, C. Zhang, Q. Liu, C. Wang, Z.-Y. Li, X. Wu and Y. Xiong, *Angew. Chem., Int. Ed.*, 2014, **54**, 2425; (*b*) L. Peng, J. Zhang, J. Li, B. Han, Z. Xue and G. Yang, *Angew. Chem., Int. Ed.*, 2013, **52**, 1792.

16 (*a*) D. Deng, Y. Yang, Y. Gong, Y. Li, X. Xu and Y. Wang, *Green Chem.*, 2013, **15**, 2525; (*b*) K. H. Lee, B. Lee, K. R. Lee, M. H. Yi and N. H. Hur, *Chem. Commun.*, 2012, **48**, 4414; (*c*) P. Zhang, J. Yuan, T.-P. Fellinger, M. Antonietti, H. Li and Y. Wang, *Angew. Chem., Int. Ed.*, 2013, **52**, 6028; (*d*) L. Peng, J. Zhang, S. Yang, B. Han, X. Sang, C. Liu and G. Yang, *Green Chem.*, 2015, **17**, 4178.

17 (*a*) J. Mitra, X. Zhou and T. Rauchfuss, *Green Chem.*, 2015, **17**, 307; (*b*) S. H. Pang, C. A. Schoenbaum, D. K. Schwartz and J. W. Medlin, *ACS Catal.*, 2014, **4**, 3123.

18 (*a*) N. Job, M. F. R. Pereira, S. Lambert, A. Cabiac, G. Delahay, J.-F. Colomer, J. Marien, J. L. Figueiredo and J.-P. Pirard, *J. Catal.*, 2006, **240**, 160; (*b*) X.-w. Cheng, Q.-y. Meng, J.-Y. Chen and Y.-c. Long, *Microporous Mesoporous Mater.*, 2012, **153**, 198.

19 W. H. Chong, L. K. Chin, R. L. S. Tan, H. Wang, A. Q. Liu and H. Chen, *Angew. Chem., Int. Ed.*, 2013, **52**, 8570.

